velocity u_v occurs at the viscous sublayer edge y_v, which is assumed to be located by

$$y^+ = u_\tau y_v / \nu_\omega = 10 \quad (8)$$

It is further assumed that the following law holds good in the viscous sublayer $u^+ = y^+$, which gives

$$u_v = \tau_\omega y_v / \mu_\omega \quad (9)$$

Equations (1), (2), (4), and (7-9) are solved, together with the perfect gas law and the Sutherland viscosity equation, to yield y_v, u_v, T_w, ρ_ω, μ_w, and τ_w.

Results and Discussion

The Reynolds-averaged Navier-Stokes equations are solved using MacCormack's implicit scheme[1] to simulate numerically shock/turbulent boundary-layer interaction. The results are obtained by integrating to the wall (ITW), as well as with wall function approach (WFA), for the following test case: $M_\infty = 2.0$, $Re_L = 0.296 \times 10^6$, and $\theta_s = 32.585$ deg (incident shock angle with the X direction). The wall is considered adiabatic. In the present test case, which is the same as the one considered by MacCormack,[8] the boundary layer does not separate as a result of interaction with the shock.

In ITW, the mesh required 32×32 grid points with 16 points in the boundary layer. The WFA required only 32×26 grid points with 10 grid points in the boundary layer—about 20% reduction in the number of grid points compared with the first case. In both cases, the starting CFL number is as high as 10, which is gradually reduced as the convergence is approached to avoid possible steady-state solution dependence on time increment Δt.[9]

The wall pressure and skin friction obtained with ITW and WFA are presented in Fig. 2. The corresponding velocity profile at $X = 4.804 \times 10^{-2}$ m are compared in Fig. 3. The figures reveal that the results obtained with the wall function approach are in good agreement with those obtained with integration to the wall.

The results of this study were obtained on a CDC Cyber 170/730 computer. It took about 25 min of CPU time to obtain converged solution with integration to the wall, while the wall function approach required about 15 min of CPU time.

In conclusion, the wall function formulation presented has been shown to result in substantial saving in computation time and storage requirements compared with integration to the wall, without significantly affecting the accuracy of the solution.

References

[1]MacCormack, R. W., "A Numerical Method for Solving the Equations of Compressible Viscous Flow," *AIAA Journal*, Vol. 20, Sept. 1982, pp. 1275-1281.

[2]Beam, R. M. and Warming, R. F., "An Implicit Factored Scheme for the Compressible Navier-Stokes Equations," *AIAA Journal*, Vol. 16, April 1978, pp. 393-402.

[3]Launder, B. E. and Spalding, D. B., "The Numerical Computation of Turbulent Flows," *Computer Methods in Applied Mechanics and Engineering*, Vol. 3, 1974, pp. 269-289.

[4]Chieng, C. C. and Launder, B. E., "On the Calculation of Turbulent Heat Transfer Downstream from an Abrupt Pipe Expansion," *Numerical Heat Transfer*, Vol. 3, 1980, pp. 189-207.

[5]Rubesin, M. W. and Viegas, J. R., "A Critical Examination of the Use of Wall Functions as Boundary Conditions in Aerodynamic Calculations," presented at Third Symposium on Numerical and Physical Aspects of Aerodynamic Flows, California State University, Long Beach, Jan. 20-24, 1985.

[6]Nakayama, A. and Koyama, H., "A Wall Law for Turbulent Boundary Layers in Adverse Pressure Gradients," *AIAA Journal*, Vol. 22, Oct. 1984, pp. 1386-1389.

[7]Hopkins, E. J., Keener, E. R., Polek, T. E., and Dwyer, H. A., "Hypersonic Turbulent Skin Friction and Boundary Layer Profiles Measured on Nonadiabatic Flat Plates," *AIAA Journal*, Vol. 10, Jan. 1972, pp. 40-48.

[8]MacCormack, R. W., "Numerical Methods for Compressible Viscous Flows," presented at the Workshop-cum-Seminar on Computational Fluid Dynamics, Vikram Sarabhai Space Centre, Trivandrum, India, Dec. 14-21, 1981.

[9]Gupta, R. N., Gnoffo, P. A., and MacCormack, R. W., "A Viscous Shock-Layer Flowfield Analysis by an Explicit-Implicit Method," NASA TM 84668, May 1983.

Nonuniform Nozzle Flow Effects on Base Pressure at Supersonic Flight Speeds

A. L. Addy,* J. C. Dutton,† and V. A. Amatucci‡
University of Illinois at Urbana-Champaign
Urbana, Illinois

Introduction

ANALYTICAL investigations of missile base flow during powered flight at supersonic speeds are principally based on one of the computer implementations of the Chapman-Korst component flow model.[1-3] To improve agreement with experiments, empirical modifications of this analysis are usually used based on small-scale experimental results. In the component model, the propulsive nozzle is generally represented as an ideal nozzle which produces either uniform or conical flow at the nozzle exit. However, many of the small-scale experiments and full-scale prototypes employ nozzle geometries which have a small radius of curvature of the throat wall, a conical expansion section with a relatively large divergence angle, and/or a truncated expansion section. These nozzles would be expected to produce nonuniform and nonconical flow at the exit, thereby affecting the plume expansion into the base region. These effects have often been hypothesized as some of the possible causes of the disagreement between the component model predictions and experimental results, although no systematic investigation of their significance on base flow has been reported. The purpose of this paper is to present parametric results of nonuniform nozzle flow effects on base pressure for typical conical nozzle geometries in order to determine their expected magnitudes and to test the hypothesis stated.

Method of Analysis

The missile base configuration under consideration is shown in Fig. 1. The internal nozzle flow expands through a conical nozzle with a circular arc throat to supersonic conditions at the exit. The nozzle geometry is completely specified by the dimensionless throat wall radius of curvature R_{CW}/R_T, by the nozzle exit radius ratio R_I/R_T, and by the divergence half-angle β_I. The external freestream flow is also assumed to be supersonic, and for the cylindrical afterbody considered, the only pertinent geometric variable is the base radius ratio R_I/R_E. The freestream and nozzle flows separate at the base and expand or compress, as the case may be, to a common base pressure P_B. A recompression

Received July 29, 1985.

*Professor and Associate Head, Department of Mechanical and Industrial Engineering. Associate Fellow AIAA.

†Associate Professor, Department of Mechanical and Industrial Engineering. Member AIAA.

‡Graduate Research Assistant, Department of Mechanical and Industrial Engineering. Student Member AIAA.

shock system forms downstream at the confluence of the separated freestream and nozzle flows.

As opposed to earlier implementations[2,3] of the Chapman-Korst flow model, which assume ideal uniform or conical nozzle flow, the present method predicts the actual nonuniform flowfield of the nozzle in Fig. 1. The approximate throat flow series solution of Ref. 4 is used to establish an initial value line for a method of characteristics calculation of the flow in the nozzle diverging section. The analysis of Ref. 4 has been compared to experimental data[4,5] and has been found to be in good agreement through a wide region of the nozzle throat. In addition, Fujii and Kutler[6] have used it to initiate finite difference nozzle flow calculations which agree well with single-phase experimental data. The start line employed here was obtained from the TRANNOZ computer code,[7] where the line used is the contour of zero radial velocity, $V(X,R)=0$. This noncharacteristic curve originates from the throat wall location, $(0,R_T)$, where the flow is supersonic and terminates on the nozzle axis at a location selected such that the local Mach number is slightly supersonic. With this technique, nozzles with a dimensionless throat wall radius of curvature as small as approximately $R_{CW}/R_T=0.5$ can be analyzed.

As shown in Fig. 1, the nozzle flowfield is calculated by the method of characteristics from the noncharacteristic starting curve to the right-running characteristic through the throat wall location. Next the flowfield is calculated for the remainder of the circular arc throat section and then for the conical diverging section. In this latter region, wave coalescence occurs and intensifies near the axis. This coalescence leads to the formation of oblique shock waves within the nozzle flowfield. Since these waves are weak, however, they can be treated approximately as the coalescence of reversible compression waves.

The base flow is predicted with the widely used TSABPP[1-3] computer implementation of the Chapman-Korst component model. In this investigation, a uniform freestream flow is assumed to approach a cylindrical afterbody, where it separates at the base. The resulting inviscid freestream constant-pressure boundary is calculated by the method of characteristics from the local freestream flow conditions M_E and P_E at the base plane and the assumed value of P_B. Similarly, the separated nozzle flow constant-pressure boundary is calculated by the method of characteristics from the local flow conditions along the nozzle exit lip characteristic c in Fig. 1 and the assumed value of P_B. The conditions along this characteristic are obtained from the nozzle flow analysis discussed previously.

In the Chapman-Korst model, the solution value of P_B is determined by linking these inviscid components to mixing components through a suitable recompression criterion at the confluence of the separated freestream and nozzle flows. The turbulent mixing layers are analyzed by means of an approximate constant-pressure mixing theory resulting in an error function velocity profile. This profile is superimposed on each of the inviscid boundaries and is localized relative to these boundaries by momentum considerations. Once the mixing profiles have been located, two important streamlines within each mixing region are determined. The first is the jet boundary streamline, which divides the separated freestream or nozzle flow from the recirculating base flow. The second is the discriminating streamline in each mixing region, which has sufficient energy, based on a recompression criterion, to match the recompression pressure rise at the confluence of the separated flows.

The recompression criterion assumes that the discriminating streamline in each mixing profile stagnates through essentially an isentropic process to the static pressure maintained by the oblique shock system downstream of the confluence of the inviscid boundaries. The recompression process in the base flow analysis is an important component which significantly affects the resulting base flow solution. However, since it is poorly understood, empirical modifications to the recompression model are often used to bring the simplified component model predictions into better agreement with experimental measurements. Once the jet boundary and discriminating streamlines have been identified in each mixing region, conservation of mass and energy in the base region provide the criteria for determining the solution values of the base pressure and temperature.

The foregoing series solution-method of characteristics-component model methodology is computationally efficient, thereby providing a means for quickly analyzing the effect of many parameters, including nozzle geometry, on the base pressure. A typical nozzle flow and base flow solution requires approximately 5 s of execution time on a CDC Cyber 175 computer.

Results and Discussion

For purposes of comparison, the nozzle flowfield was calculated for the same conical nozzle analyzed by Fujii and Kutler[6] for single-phase flow; this nozzle has $R_{CW}/R_T=0.625$, $R_I/R_T=2.625$, and $\beta_I=15$ deg. This configuration has also been analyzed by Serra[8] and experimentally investigated by Back and Cuffel.[9] The wall and axis Mach number distributions due to Fujii and Kutler, Serra, and Back and Cuffel (taken from Fig. 2 of Ref. 6) are compared to the results of the present nozzle analysis in Fig. 2. The present method agrees quite well with both the measurements and the results of Fujii and Kutler for the wall Mach number distribution. All three analytical techniques also predict the axis Mach number profile reasonably well up to the point where the steep decrease in the Mach number occurs after

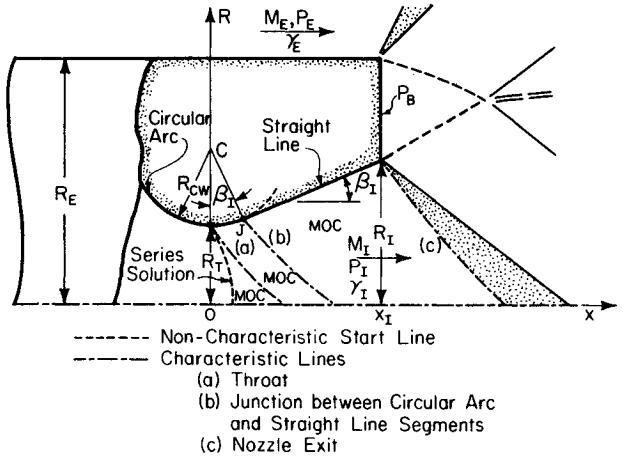

Fig. 1 Missile base configuration and nomenclature.

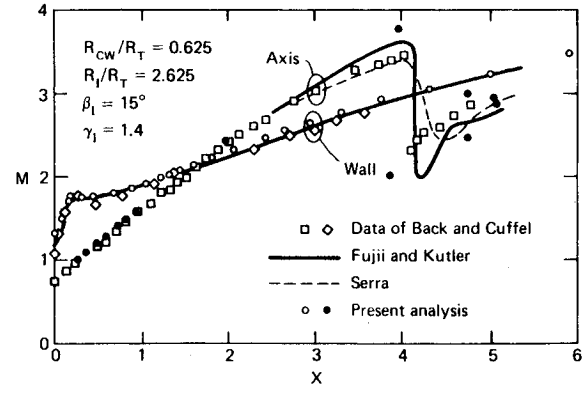

Fig. 2 Comparison of the present conical nozzle flowfield analysis with the analyses and experiments of others.

the onset of compression on the axis. At this point the various analyses and data diverge somewhat, although it appears that the present technique predicts the axis Mach numbers at least as well as the two finite-difference methods. Since this nozzle configuration represents an extreme geometry and the present analysis provides generally good agreement with other prediction methods and experimental data, the present method is considered to be adequate for the current study.

For the base flow investigation, the conical nozzle exit radius ratio and divergence half-angle were fixed at $R_I/R_T = 1.6239$ and $\beta_I = 15$ deg, respectively. The parametric values considered for the dimensionless throat wall radius of curvature were $R_{CW}/R_T = 0.75$, 1.0, 1.5, 2.0, 4.0, and 8.0 and for the nozzle gas specific heat ratio were $\gamma_I = 1.25$ and 1.4. Since R_{CW}/R_T was varied but R_I/R_T was held constant, the dimensionless length of the nozzle varies directly with the throat wall radius of curvature ratio. Also, the exit radius ratio value corresponds to a nominal exit Mach number of $M_I = 2.343$ for $\gamma_I = 1.25$ and $M_I = 2.5$ for $\gamma_I = 1.4$. The base thickness radius ratio was taken as $R_I/R_E = 0.6$ and, for purposes of comparison with earlier parametric results with ideal conical nozzles,[3] the freestream flow parameters were also fixed at $M_E = 2.0$ and $\gamma_E = 1.4$.

Figure 3 presents the base pressure results for $\gamma_I = 1.4$ over the operating pressure ratio range $2 \le P_I/P_E \le 8$. The top line in Fig. 3 gives the base pressure ratio P_B/P_E over this range as predicted by the original Chapman-Korst component flow model assuming ideal conical nozzle flow and without any of the empirical modifications which are used to bring the theory and experimental measurements into closer agreement. The calculations embodied in this line serve as the baseline case for determining whether or not nonuniform nozzle flow effects are a major source of the discrepancy between the original theory and experiments and what the magnitudes of these effects are. The percent deviations Δ from the baseline case are plotted in the central portion of Fig. 3 for each of the parametric values of R_{CW}/R_T, where

$$\Delta \text{ (percent)} = \frac{100[(P_B/P_E) - (P_B/P_E)_{\text{baseline}}]}{(P_B/P_E)_{\text{baseline}}}$$

As can be seen, nonuniform nozzle flow effects result in a maximum *increase* in base pressure of approximately 6%, and, interestingly, this maximum deviation occurs at the intermediate radius of curvature ratio $R_{CW}/R_T = 1.5$. This latter result can be explained as follows. For $R_{CW}/R_T = 8.0$, the nozzle flowfield nonuniformities introduced by the throat geometry are small so that the base pressure deviation from the ideal conical case is also small. As R_{CW}/R_T is decreased, the throat flow nonuniformities become more pronounced and Δ increases as a result. However, as R_{CW}/R_T is reduced further, a competing effect appears. Since the exit radius R_I/R_E is constant, the conical divergent section of the nozzle (point J to the exit in Fig. 1) is longer for these smaller values of R_{CW}/R_T. Therefore, even though larger flowfield nonuniformities are introduced by these sharp throat curvatures, the flow has a larger distance over which to relax back toward ideal conical conditions. As a result, Δ decreases again. The base pressure results for $\gamma_I = 1.25$ (not shown) are qualitatively similar to those for the $\gamma_I = 1.4$ case presented in Fig. 3. However, the maximum deviation is approximately 7% and occurs for $R_{CW}/R_T = 1.0$.

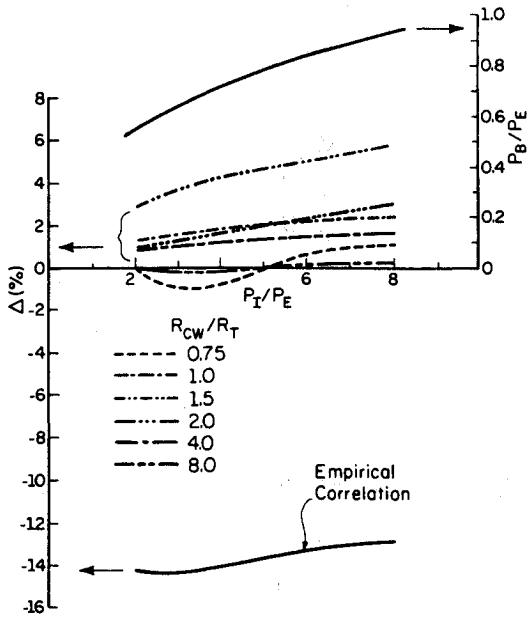

Fig. 3 Base pressure results for $\gamma_I = 1.4$.

Also shown in Fig. 3 are component model calculations which utilize the empirical recompression criterion proposed in Ref. 10. However, for the purposes of the present discussion, this line may be considered simply as an empirical correlation of the approximately 150 experimental data sets which form the basis of this criterion. Since the component model with nonuniform nozzle flow effects included generally predicts a *higher* base pressure than the ideal conical flow baseline case while the experimental measurements fall 13-14% *below* this same baseline, it is readily concluded that these effects are *not* the primary source of the disagreement between the original unmodified component model and experiments. In fact, these results point out that there must be other, larger factors not accounted for in the original theory which act in the opposite direction to bring the base pressure down to the measured level. Such factors include the afterbody and nozzle wall boundary layers and inadequate modeling of the mixing, recompression, and redevelopment processes. In addition, since experimental and prototype hardware often have nozzle geometries for which the present analysis predicts significant nonuniform nozzle flow effects on the base flow, these effects should be included in the development of more advanced component models or in Navier-Stokes flowfield calculations. Only when all pertinent mechanisms are understood and properly treated will a unified, nonempirical base flow theory be realized.

Acknowledgments

This research was sponsored in part by the U. S. Army Research Office under Contract DAAG 29-79-C-0184 and the Department of Mechanical and Industrial Engineering.

References

[1]Addy, A. L., "Detailed Analyses for the Base-Pressure Programs (TSABPP-1,2)," U. S. Army Missile Command, Redstone Arsenal, AL, Rept. RD-TN-69-7, Aug. 1969.

[2]Addy, A. L., "Analysis of the Axisymmetric Base-Pressure and Base-Temperature Problem with Supersonic Interacting Freestream-Nozzle Flows Based on the Flow Model of Korst, et al., Part I: A Computer Program and Representative Results for Cylindrical Afterbodies," U. S. Army Missile Command, Redstone Arsenal, AL, Rept. RD-TR-69-12, July 1969.

[3]Addy, A. L., "Analysis of the Axisymmetric Base-Pressure and Base-Temperature Problem with Supersonic Interacting Freestream-Nozzle Flows Based on the Flow Model of Korst, et al., Part III: A Computer Program and Representative Results for Cylindrical, Boattailed, or Flared Afterbodies," U. S. Army Missile Command, Redstone Arsenal, AL, Rept. RD-TR-69-14, Feb. 1970.

[4]Dutton, J. C. and Addy, A. L., "Transonic Flow in the Throat Region of Axisymmetric Nozzles," *AIAA Journal*, Vol. 19, June 1981, pp. 801-804.

[5]Dutton, J. C. and Addy, A. L., "Transonic Flow in the Throat Region of Annular Supersonic Nozzles," *AIAA Journal*, Vol. 20, Sept. 1982, pp. 1236-1243.

[6]Fujii, K. and Kutler, P., "Computations of Two-Phase Supersonic Nozzle Flows by a Space-Marching Method," AIAA Paper No. 83-0041, Jan. 1983.

[7]Dutton, J. C. and Addy, A. L., "TRANNOZ: A Computer Program for Analysis of Transonic Throat Flow in Axisymmetric, Planar, and Annular Supersonic Nozzles," Department of Mechanical and Industrial Engineering, University of Illinois at Urbana-Champaign, Rept. UILU-ENG-80-4005, April 1980.

[8]Serra, R. A., "Determination of Internal Gas Flows by a Transient Numerical Technique," *AIAA Journal*, Vol. 10, May 1972, pp. 603-611.

[9]Back, L. H. and Cuffel, R. F., "Detection of Oblique Shocks in a Conical Nozzle with a Circular-Arc Throat," *AIAA Journal*, Vol. 4, Dec. 1966, pp. 2219-2220.

[10]Addy, A. L., "Experimental-Theoretical Correlation of Supersonic Jet-On Base Pressure for Cylindrical Afterbodies," *Journal of Aircraft*, Vol. 7, Sept.-Oct. 1970, pp. 474-477.

Swirl Generator for Independent Variation of Swirl and Velocity Profile

W. L. H. Hallett*
University of Ottawa, Ottawa, Canada

Introduction

A SWIRL generator that allows both the swirl parameter and the shape of the axial velocity profile at the swirler exit to be varied independently, was devised for some recent studies of the effects of inlet conditions on the occurrence of central backflow in swirling flow. Figure 1 shows the essential features of the design. Swirl is produced by admitting air through four tangential entries, whose length L may be varied by means of a sliding sleeve, thus controlling the angular momentum imparted to the flow. To achieve a uniform inlet velocity, each tangential duct is provided with a movable partition attached to the sleeve and a bell-mounted entry. A second, nonswirling stream enters through a central tube, reducing the swirl intensity of the resulting flow. By regulating the proportions of air introduced tangentially and axially as well as the inlet length L, both the swirl intensity and the shape of the axial velocity profile at the swirler exit can be varied. The principle of combining axial and tangential streams is well known as a means of controlling swirl,[1-4] but has not previously been employed for the expressed purpose of velocity profile variation as well.

Measurement of Performance

The velocity profiles produced were measured with a five-hole Pitot probe at the port shown in Fig. 1. During these tests the swirl generator discharged into a cylindrical tube of 305 mm diam, while the Reynolds number lay between 0.8×10^6 and 2.5×10^6. The tip of the axial inlet tube was kept 10 mm forward of the end of the tangential inlet for all L settings (Fig. 1). Operating conditions are specified by the inlet length L and the ratio ξ

$$\xi=\dot{m}_t/(\dot{m}_t+\dot{m}_a) \tag{1}$$

where $\dot{m}_t$ and $\dot{m}_a$ are the tangential and axial mass flows, respectively. The outlet flow is characterized by the dimensionless angular momentum flux Ω,

$$\Omega=\frac{2\pi}{RI}\int_0^R \rho u w r^2 dr \tag{2}$$

where u and w are the measured local axial and tangential velocities, respectively, r the radius, ρ the density, and I a momentum flux based on the mean axial velocity $\bar{u}$:

$$I=\pi R^2\rho\bar{u}^2 \tag{3}$$

where

$$\bar{u}=(\dot{m}_t+\dot{m}_a)/\rho\pi R^2 \tag{4}$$

Evaluation of $\bar{u}$ by integration of the velocity data eliminated most measurement error from Ω.

Figure 2 plots the measured Ω as a function of L and ξ, while Fig. 3 indicates the degree to which velocity profile shapes can be varied at approximately constant Ω. The unsteady flow region marked in Fig. 2, discovered by flow visualization with smoke, is probably caused by vortex shedding in the wake of the central tube, which behaves as a bluff body as $\dot{m}_a$ approaches 0. The position of the axial inlet tube was found to have some effect on angular momentum flux, a position further forward than that shown in Fig. 1 giving a slightly higher Ω, especially at high ξ and small L.

Correlation of Angular Momentum Flux

The usual means of calculating the angular momentum flux produced by a tangential entry assumes a uniform velocity u_t in the n entry ducts,[4,5] giving

$$\Omega=\frac{\dot{m}_t u_t e}{IR}=\frac{\dot{m}_t^2 e}{\rho nbLIR} \tag{5}$$

where

$$e=R-b/2 \tag{6}$$

The swirler was found to produce a higher Ω than predicted by Eq. (5), suggesting that the jet leaving each entry undergoes contraction and acceleration as it combines with flow from preceding entries. To describe this, a contraction coefficient C_c is introduced, so that

$$u_t=\frac{\dot{m}_t}{\rho nbLC_c} \tag{7}$$

Frictional losses of angular momentum are equal to the torque T exerted by the tube wall,

$$T=2\pi\tau_\phi R^2 X \tag{8}$$

with the shear stress expressed as

$$\tau_\phi=f_\phi\rho u_t^2/8 \tag{9}$$

where f_ϕ is a friction factor, analogous to that in simple pipe flow, and u_t is assumed to be typical of tangential velocities near the wall. Combining Eqs. (4), (5), and (7) and subtract-

Received Aug. 30, 1985.

*Assistant Professor, Department of Mechanical Engineering.